

MAPPING OF THE STRUCTURE OF THE GALACTIC MAGNETIC FIELD WITH VELOCITY GRADIENTS: TEST USING STAR LIGHT POLARIZATION

DIEGO F. GONZÁLEZ-CASANOVA AND A. LAZARIAN

Astronomy Department, University of Wisconsin-Madison, 475 North Charter Street, Madison, WI 53706-1582, USA

Draft version May 11, 2022

ABSTRACT

We apply Velocity Channel Gradients (VChGs) and Reduced Velocity Centroids Gradients (RVCGs) to HI data (the LAB survey) and get the plane of the sky component of the magnetic field as a function of the relative velocity. Assuming a galactic rotation curve, we transformed the relative velocities to distances, constructing the first map of the galactic 3D magnetic field. To test the accuracy of our 3D distribution we used a set of stars with known distances from the stellar polarization (Heiles 2000) catalog and compared the polarization directions that we obtain with our 3D magnetic field map with the actual starlight polarization directions. We find a good correspondence between the expected and measured polarization directions which testify of the accuracy of the new way of probing the 3D galactic magnetic field structure.

Subject headings: ISM: magnetic fields, kinematics and dynamics - turbulence - methods: observational

1. INTRODUCTION

Magnetic fields and turbulence are ubiquitous in the interstellar medium (ISM), acting as important drivers of galaxy evolution and feedback mechanisms. In the ISM, they significantly affect key astrophysical phenomena such as star formation, cosmic ray acceleration and propagation and feedback mechanisms (Elmegreen & Scalo 2004; McKee & Ostriker 2007; Crutcher 2012; Naab & Ostriker 2016). Their effects are imprinted in electron density fluctuations, anisotropies of spectroscopic data, and Doppler broadening, to name a few situations (Armstrong et al. 1995; Chepurnov & Lazarian 2010; Lazarian & Pogosyan 2000). It is therefore fundamental to understand the strength and direction of the magnetic field in the ISM, as well as its morphology across the entire galaxy.

Zeeman splitting (see Crutcher et al. 2010) provides the most detailed information about the line of sight magnetic field in the interstellar medium. The measurements are very time consuming and in most cases only upper limits of the magnetic fields are obtained. Far infrared polarimetry of aligned dust (see Andersson et al. 2015) provides the 2D maps of the plane of sky magnetic fields directions. *Planck* data (Planck Collaboration et al. 2016a,b) provided a revolution in our understanding of plane of the sky magnetic fields. However, to increase the resolution of the maps one has to use either balloon suborbital instruments, e.g. BLASTPOL (see Fissel et al. 2016) or wait for future space missions. By measuring the polarization from stars with the known distances (see Heiles 2000) one can get a some insight into the 3D structure of the galactic magnetic field. This way of magnetic field sampling is limited, as it is possible only to sample magnetic fields in the direction towards the stars with known distances. In addition, all dust polarimetry techniques¹ suffer from existing uncertainties related to grain alignment and the failure of grains to

align at high optical depths (see Lazarian et al. 2015, for a review).

In this paper we discuss the new technique of obtaining 3D magnetic field in atomic hydrogen that is based on the present day understanding of MHD turbulence. The technique employs both velocity gradients and galactic rotation curve to map the plan of the sky distribution of magnetic field directions.

The first paper discussing the velocity gradients as the means of magnetic field tracing was González-Casanova & Lazarian (2017, henceforth GL17). There the velocity centroids (see Esquivel & Lazarian 2005) were employed to represent the velocity information. To use velocity resolution to distinguish parts of the interstellar gas, which due to galactic rotation move at different velocities Lazarian & Yuen (2018, LY18) introduced Velocity Channel Gradients (VChGs) and Reduced Velocity Centroids Gradients (RVCGs). LY18 proposed to use both tools to find the 3D distribution of magnetic fields by employing the galactic rotation curve. Our paper is the first practical attempt to implement this idea. For our calculations we use the procedure of subblock averaging introduced in Yuen & Lazarian (2017b). The latter procedure allows us to reliably trace the gradient directions and evaluate the uncertainties of our magnetic field direction measurements.

Our tracing of directions in HI has some similarities to the procedure of filament identification in Clark et al. (2014, 2015). There it was found empirically that for high galactic latitude HI, filamentary structures can be identified in velocity channel maps and these filaments tend to align with the magnetic field as measured by Planck polarimetry. We believe that the measured filaments are mostly velocity caustics rather than the real density structures. This follows from the theory of the statistics of fluctuations in the Position-Position-Velocity (PPV) space formulated in Lazarian & Pogosyan (2000) (see also Lazarian 2009, for a review). In our view the observed “filaments” and the gradients in velocity channel maps that we employ within the VChG technique both measure the properties of turbulent velocities. We shall

casanova, lazarian @ astro.wisc.edu

¹ Instrumental polarimetry is another curse of the polarimetry measurements.

provide a detailed comparison of the two ways of magnetic field tracing elsewhere and will mention in passing that for denser regions, e.g. molecular clouds, the filamentary structure in channel maps fades away and gets not measurable but velocity gradients can still trace magnetic field reliably (see LY18).

Our approach should not be confused with using density gradients within the Histograms of Relative Orientation technique (HRO) (Soler et al. 2013, 2017). The HRO is designed to compare the direction of density gradients and magnetic field as a function of column density. It requires polarization measurements and is not intended for obtaining the magnetic field direction on its own.

The VChGs and RVCGs that we employ here are particular incarnations of the Velocity Gradient Technique (VGT) which is based on the present day understanding of MHD turbulence theory. The core paper is that on the theory of incompressible MHD turbulence by Goldreich & Sridhar (1995, henceforth GS95). This paper predicts the anisotropy of MHD turbulence. The theory of turbulent reconnection in Lazarian & Vishniac (1999, henceforth LV99) explains that eddies are not constrained from rotating perpendicular to the direction of the magnetic field that surrounds them. Any other types of magnetic field motion are resisted by magnetic tension force. As a result, the random turbulent driving preferentially induces motions perpendicular to the magnetic field that surrounds the eddies. Incidentally, this way of thinking naturally introduces the importance of *local* magnetic field in respect to which the motions of Alfvénic turbulence develop. The concept of the local system of reference was not a part of the original GS95 model of turbulence. However, that the local system of reference is essential was confirmed by numerical simulations (Cho & Vishniac 2000; Maron & Goldreich 2001). We stress that for the VGT, it is essential that turbulent eddies trace the *local* magnetic field around eddies rather than the mean magnetic field.²

It is natural to expect the Alfvénic eddies that are not constrained by magnetic tension create a Kolmogorov cascade with velocities $u_l \sim l_\perp^{1/3}$, where l_\perp is measured in respect to the local direction of magnetic field. It is also evident that the eddies mixing magnetic field lines perpendicular to their direction should induce Alfvénic waves (velocity V_A) along the magnetic field. The equality of the eddy turnover time l_\perp/u_l and the period of the Alfvén wave l_\parallel/V_A that is being induced by the eddy corresponds to the “critical balance” that can be written as:

$$l_\parallel^{-1}V_A \approx l_\perp^{-1}u_l. \quad (1)$$

It is easy to see that the predicted anisotropy of the eddies will be increasing with the decrease of the scale. Indeed, u_l decreases with the scale as $l^{1/3}$, which induces the change of the l_\perp to l_\parallel ratio.

Note, that the GS95 assumes that the velocity at the injection scale is V_A . This is the case of transAlfvénic turbulence. The anisotropy even more prominent if the

injection velocity is less than V_A , as it is quantified in LV99.

Two important observations are due. The first one is that the anisotropy is that the smaller the eddies the closer their gradients (turned 90 degrees) follow the local magnetic field direction. Furthermore, this velocity gradient, Ω , increases as the eddy sizes decreases ($\Omega \sim l_\perp^{-2/3}$). It is also possible to prove that the velocity gradients arising from the smallest eddies at the scales resolved by a telescope dominate the gradient signal in spite of the effect of the line of sight averaging (see Lazarian et al. 2018).

In this work we obtain the VChG and RVCG from HI spectroscopic data to acquire the structure of the galactic magnetic field as a function of relative velocity. The VChG and RVCG measurements are compared to stellar polarization measurements to determine the effectiveness of the technique. To compare the two measurements we use the galactic rotation curve to relate the distances to velocities, allowing a direct comparison (at least on the plane of the galaxy). We then derived a map of the structure of the perpendicular component of the galactic magnetic as a function of distance.

In Section 2, we describe the different surveys used; in Section 3, we describe the method used; in Section 4, we present the VChG and RVCG analysis on the HI data and the alignment with stellar polarization; in Section 5, we present the structure of the magnetic field in the galaxy and how it relates to ; and in Section 6, we discuss the impacts of the magnetic field map; in Section 7, we give our conclusions.

2. OBSERVATIONAL DATA

2.1. *Hi data*

The HI data used comes from the Leiden/Argentine/Bonn (LAB) Survey (Kalberla et al. 2005). The LAB survey is a combination of two independent HI surveys, that together represent the first HI map of the entire sky. The LAB Survey is the most sensitive full sky survey kinematically. The LAB survey merges the Leiden/Dwingeloo survey ($\delta \geq -30^\circ$) (Hartmann & Burton 1997) with the Instituto Argentino de Radioastronomía Survey (Arnal et al. 2000; Bajaja et al. 2005) ($\delta \leq -25^\circ$). The spectral resolution is 1.3 km s^{-1} and the velocity coverage is 850 km s^{-1} ($-450 \text{ km s}^{-1} < v_{LSR} < 400 \text{ km s}^{-1}$) with an angular resolution of $30'$ and $35.7'$ for the southern and northern parts respectively.

2.2. *Star polarization data*

The measures of starlight polarization come from the Heiles (2000) catalog, a compilation of 9286 Stars. This catalog attempts to eliminate errors, provide positions, weight multiple observations of the same star, and provide distances to the stars. The stars in the catalog are located across the whole sky but primarily in the plane of the galaxy.

We only use polarization data from stars for which distances were measured with *Hipparcos* and found to be less than 4 kpc away. The 4 kpc radius limit represents the maximum distance *Hipparcos* can measure (Perryman et al. 1997; Heiles 2000). This increases the accuracy of the distance measurements, enabling us to better

² All earlier MHD turbulence theories, including the original formulation of the GS95 theory were done in respect to the mean field. The GS95 relations, however, are valid only in the local system of reference.

compare the different observations. We further constrain the sample to only those stars where the polarization percentage is $pp \geq 0.9$, as defined in Heiles (2000) below:

$$pp = \sqrt{\langle Q \rangle^2 + \langle U \rangle^2}, \quad (2)$$

where $\langle Q \rangle$ and $\langle U \rangle$ are the Stokes parameters for each star. We use the polarization percentage of 0.9 to increase the alignment between the star polarization and the inferred magnetic field. With the polarization and distance constraints there are 1139 stars in the sample.

3. METHOD

Using the spectroscopic HI data we constructed velocity channel maps LY18 and used two different techniques to calculate the velocity gradients, namely the VChG and RVCG. To obtain the VChGs, the channel maps are formed with thin channels in the way defined by Lazarian & Pogosyan (2000), since intensity fluctuations within thin channels represent velocity fluctuations rather than those induced by turbulent density (see Lazarian & Pogosyan 2000). This procedure calculates the gradient at each of the channels using the sub-block averaging procedure in YL17. This is the way that we obtain the plane of the sky (POS) magnetic field at each channel.

The second approach used, is the reduce velocity centroid gradients (RVCG) the gradients are obtain in thicker velocity channels than the VChG but of the velocity centroid, S , rather that of the intensity. The RVCG covers all the the velocity rage of the data, and its also dependent on the line of sight (LOS) velocity (just like the VChG). The RVCG and the VChG where found to have the same type of alignments between our inferred magnetic field direction and the one form polarization measurements, therefore for the rest of the paper we will be only showing the results form the RVCG.

The procedure of sub-block averaging in YL17 allows us to calculated both gradients with higher accuracy. In practical terms, the gradients are calculated similarly to VCG, but on each of the slices of the velocity/intensity channel map for RVCG and VChG respectively. Each slice is interpolated using the bi-cubic spline approximation over a rectangular mesh, adding 10 extra cells between each of the original points. At each of the original cells and for each slice, the direction of the gradient that indicates the magnetic field is in the direction of the cell that maximizes $\nabla^S(\mathbf{X}, v_z)$ with:

$$\nabla^S(\mathbf{X}, v_z) = \frac{|S(\mathbf{X}, v_z) - S(\mathbf{X} + \mathbf{X}', v_z)|}{|\mathbf{X}'|}, \quad (3)$$

where \mathbf{X} and \mathbf{X}' are points in the POS, S is the intensity at the thin channel that mimics the velocity or the reduce velocity centroid, and v_z is the center velocity for each slice of the velocity centroid channel map. \mathbf{X}' is defined in an annulus with a radius of 10 cells around \mathbf{X} .

The Gaussian fitting YL17 procedure enhances the accuracy of the technique compared to its original implementation of GL17 by allowing more cell (angle) possibilities to find the maximum gradient due to the interpolation process. The accuracy of the Gaussian fitting allows to evaluate the precision of magnetic field tracing. At the same time, the properties of the Gaussian can be

used to determine the media magnetization given by the Alfvén Mach number (Lazarian et al. 2018).

The aforementioned procedure uses the statistical nature of the data and divides the data into blocks for each of the slices. In our case the blocks are 21^2 cells each (or $\sim 10.5^\circ$). At each block, the most common direction of the gradient is determined and assigned to each block. This procedure increases the alignment of the technique while losing spatial resolution. This procedure was tested on GALFA-HI DR1 survey and the alignment was corroborated with *Planck* data. We also compare our results to the *Planck* data by binning the data to the same resolution as the HI data YL17.

For our work we use four values (20 km s^{-1} , 10 km s^{-1} , 5 km s^{-1} and 2.5 km s^{-1}) for the channel widths when constructing the velocity channel maps for the RVCG and the 2.5 km s^{-1} for the VChG. The velocity range used is -123 km s^{-1} to 156 km s^{-1} , covering the *Hip-parcos* instrument-limited 4 kpc radius around the sun used for our measurements. Future measurements from *Gaia* will provide higher precision estimations on the distances, which will allow us to extend this analysis to greater distances and in particular out of the plane of the galaxy (Gaia Collaboration et al. 2018; Luri et al. 2018).

4. VELOCITY GRADIENT ANALYSIS AND THE ALIGNMENT WITH STAR POLARIZATION

The stellar polarization direction corresponds to the LOS integrated direction from the observer to the star. The magnetic field direction obtained with the velocity gradients corresponds to a local measurement (in velocity). The localized velocity measurement has an uncertainty arising from the turbulent velocity dispersion. To compare both measurements we first transform the position of a star in position-position-position (PPP) to position-position-velocity (PPV)³.

This transformation is done assuming a galactic rotation curve given by McClure-Griffiths & Dickey (2007):

$$V = \left(0.186 \left(\frac{R}{R_\odot} \right) + 0.887 \right) V_\odot, \quad (4)$$

where R_\odot is the distance from the Galactic Center to the Sun ($R_\odot = 8.34 \text{ kpc}$), V_\odot is the circular velocity at the Sun's location ($V_\odot = 220 \text{ km s}^{-1}$), V the circular velocity of an object ($3 \text{ kpc} < R < 8 \text{ kpc}$). After 8 kpc we assume a flat rotation curve. From the star catalog we know both the spatial coordinates and its distance. With that we can determine the velocity of the star and then the relative velocity (V_r) given by:

$$V_r = R_\odot \sin(l) \left(\frac{V}{R} - \frac{V_\odot}{R_\odot} \right). \quad (5)$$

The relative velocity is the same as the LOS velocity in the HI PPV cube. Figure 1 shows the relative velocity and polarization angle for each of the stars analyzed. Once the relative velocity is obtained, the stars

³ In contrast, in subsection 5 we transform the results form the RVCG (that are velocity dependent), in order to a distance to create a first map of the galactic magnetic field.

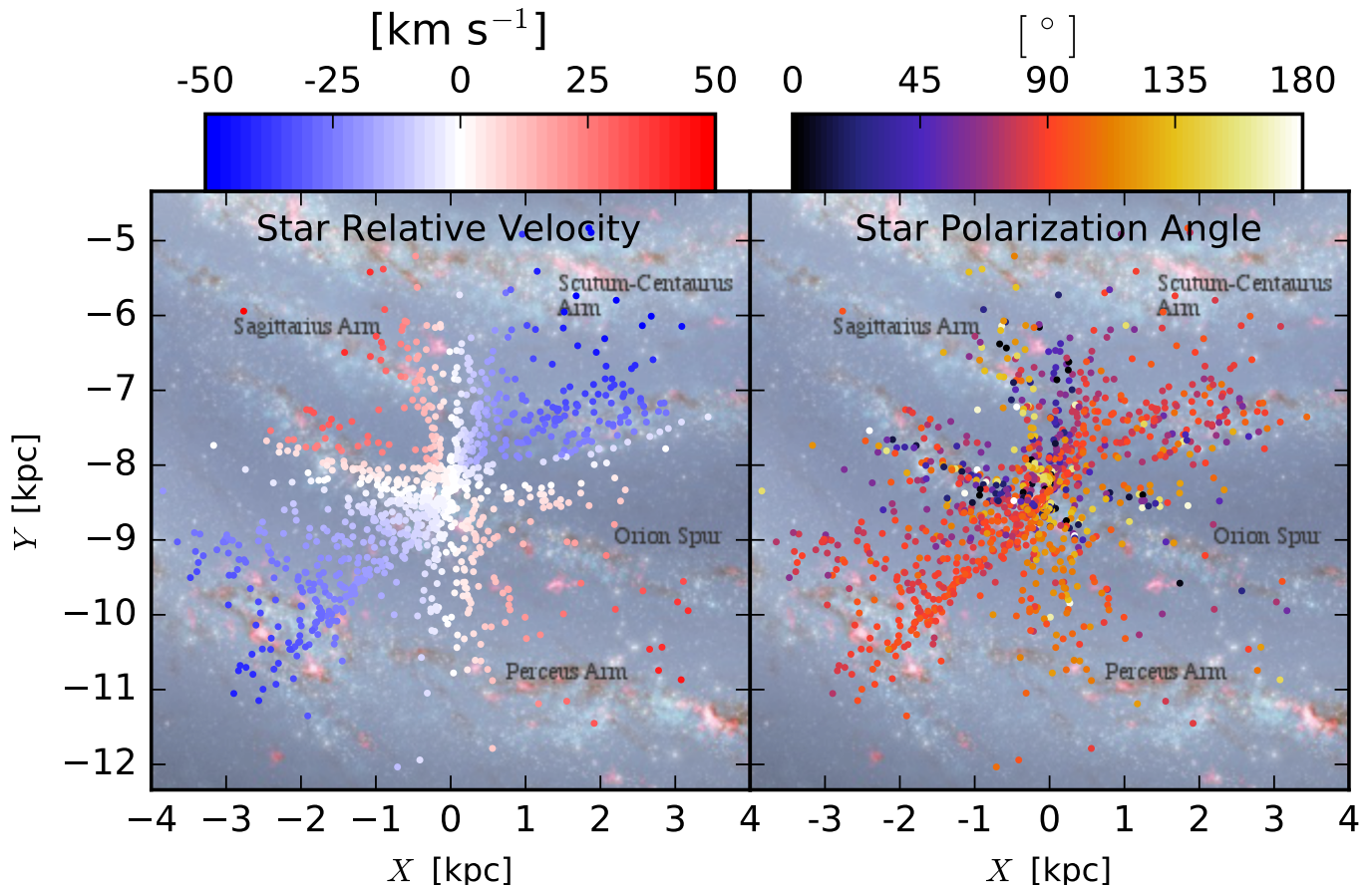


FIG. 1.— Locations of the 1139 stars analyzed in the galaxy, projected onto the plane of the galaxy. The distance, latitude, and longitude are obtained from the Heiles (2000) catalog. *Left panel* shows the relative velocity of each star assuming only circular motions. *Right panel* shows the stellar polarization angle as given in the Heiles (2000) catalog. As a background we show the Milky Way with the Scutum-Centaurus, Sagittarius, and Perseus spiral arms along with the Orion Spur where the Sun is located. The velocity has a visual limit of 50 km s^{-1} , for contrast with the Milky Way background.

are binned in different channels according to each star’s specific velocity and the thickness of the channels, to construct a PPV cube with the observed stellar polarization information. This assumes that all the stars in the stellar catalog do not have proper motion.

The conversion between distances and velocities assumes a galactic rotation curve, with a 220 km s^{-1} velocity at the solar circle. As discussed on the paper McClure-Griffiths & Dickey (2007) a different value for the velocity would not drastically change the quality of the rotation curve. Furthermore, because we worked with relative velocities there are no significant changes in the velocity estimations.

With the velocity transformation, both measurements have the same spatial relation but different magnetic field direction information. Our approach provides local measurements of the magnetic field while the stellar polarization corresponds to a LOS integrated measurement. The polarization and gradients provide different results when they are adding up. To make a better we use the procedure described in Clark (2018). We transformed the local measurements to a LOS integration, constructing the “pseudo” Q and U Stokes parameters from the directions given by velocity gradients and then integrating “pseudo-Stokes” parameters along the LOS. The difference of our study with that in Clark (2018) is that we are constructing the “pseudo-Stokes” parameters using

velocity gradients rather than filament directions of HI intensity.

In other words we use

$$\begin{aligned} Q(\mathbf{X}, v_z) &= I(\mathbf{X}, v_z) \cos(2\theta(\mathbf{X}, v_z)), \\ U(\mathbf{X}, v_z) &= I(\mathbf{X}, v_z) \sin(2\theta(\mathbf{X}, v_z)), \end{aligned}$$

where I is the HI intensity at each cell in PPV, θ is the angle of the magnetic field from the VGT. The angle that is used to compared to stellar polarization measurements is:

$$\phi = \frac{1}{2} \tan \left(\frac{\int U(\mathbf{X}, v_z) dv_z}{\int Q(\mathbf{X}, v_z) dv_z} \right), \quad (6)$$

where the velocity integration corresponds the LOS integration in velocity space. This integral could also be done in space instead of velocity.

For each star we now have the stellar polarization and the inferred magnetic field direction from the VGT in a format that we can now compare. We compared them with the alignment measure, AM (see GL17)

$$AM = 2 \left\langle \cos(\xi)^2 - \frac{1}{2} \right\rangle, \quad (7)$$

where ξ is the angle between the two vectors. The AM is well-suited to compare the alignment between two vectors as it precisely measures the properties of circular

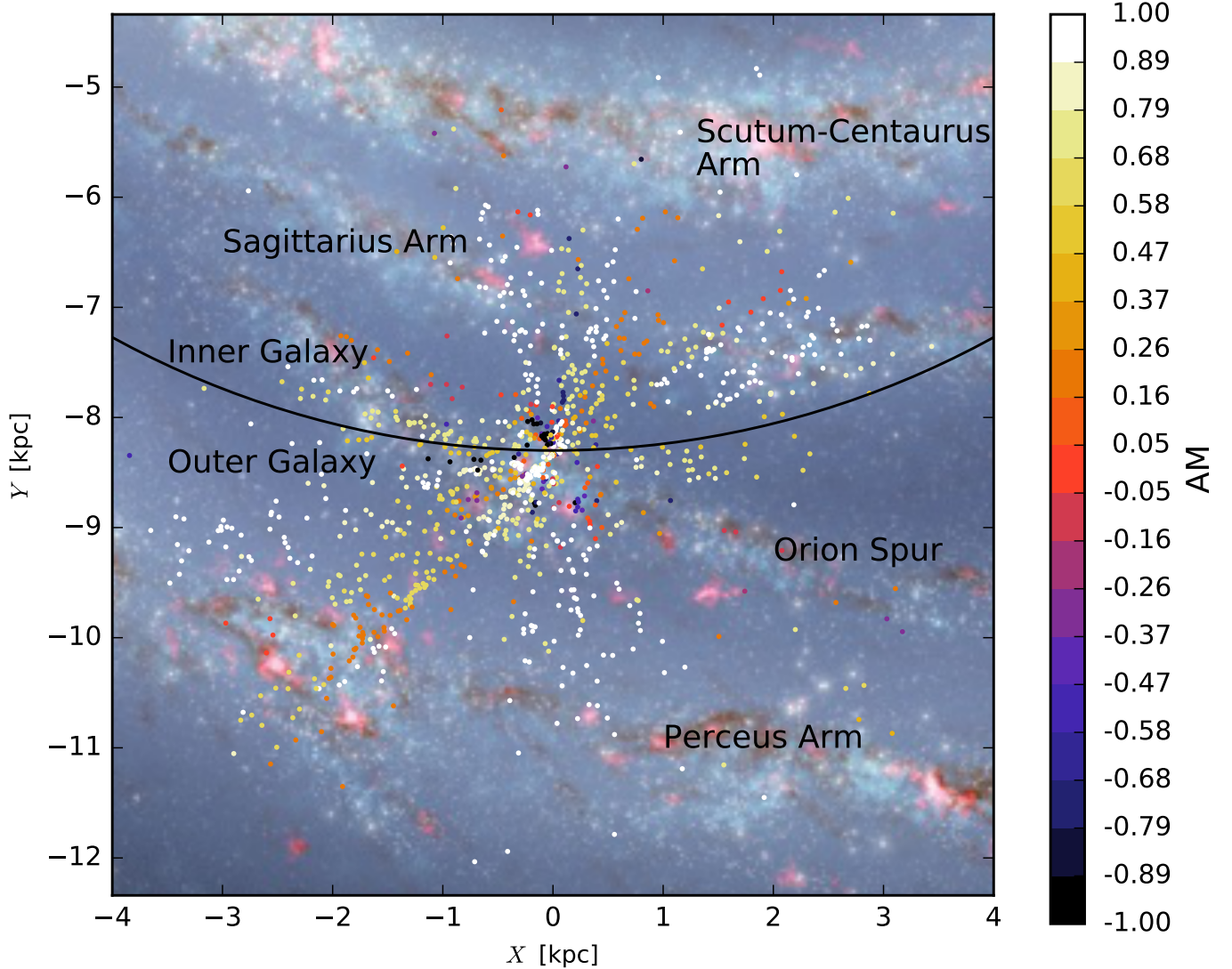


FIG. 2.— The Alignment Measure (AM) for each star between the stellar polarization and the inferred magnetic field direction for their location, showing relative location in the galaxy. We used a thickness of 10 km s^{-1} for our velocity channel using the RVCG. An AM of 1 implies a parallel configuration between the two vector measurements. The solar circle is shown, anything inside it corresponds to the inner galaxy where the distance and velocity do not have a one to one correspondence.

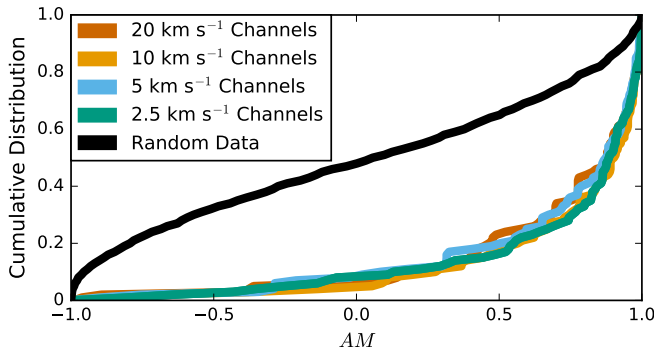


FIG. 3.— The cumulative distribution of the Alignment Measure (AM) between the stellar polarization and the inferred magnetic field from the VGT. The different colors indicate the different channel width used for the RVCG. It is clear that the alignment is similar for all the velocity thicknesses used and for all cases the mean is ≥ 0.9 . The random case in *Black* is the AM of two random vectors in the unit circle.

data (just like angle measurements). The AM is widely used in dust alignment theory. The AM ranges from -1 to

1, with $AM = 1$ for a parallel or anti-parallel configuration and $AM = -1$ for a perpendicular one.

Figure 2 shows the AM between the two measurements for the 10 km s^{-1} channel width using RVCG. Figure 3 shows the same information in a cumulative distribution but for the four different channel widths also for the RVCG and a random distribution. In general, we observe a good alignment, regardless of channel width, for most of the stars.

This is the first attempt of doing such sort of analysis and more studies are necessary. We notice, for instance that in some directions a few stars show “anti-alignment”. With better distance evaluation to stars and more star polarization measurements we are going to address these issues. *Gaia* (Gaia Collaboration et al. 2018; Luri et al. 2018) is the project that is going to provide more star distances that combined with The Galactic Plane Infrared Polarization Survey (GPIPS) Clemens et al. (2012) will provided many more starlight polarization measurements with associated distances. With the

present data we do not see an evident spatial correlation between the AM and the location of the stars, implying that the technique of magnetic field tracing is applicable to a significant part of the HI galactic disk.

It is important to note that for the I and IV galactic quadrants (in side the solar radius) the velocity information corresponds to two different spatial positions in the galactic disk. Therefore using the VGT in this quadrants gives a convoluted direction of the magnetic field, that might be incorrect. As seen in Section 5 the POS magnetic field across the galaxy does not highly deviate allowing us to suggest that the measurements in the I and IV quadrants should present the actual magnetic field. Soler et al. (2016) using *Planck* also found that the POS magnetic field comes from a local environment similar to our findings. Even with a small changing magnetic field, the average AM for the inner galaxy and for the outer one shows measurable differences. The inner galaxy AM is 0.6 while the outer part is 0.65 and the average one is 0.62 (all this for the RVCG with 10 km s^{-1} channel width).

5. 3D STRUCTURE OF THE MAGNETIC FIELD

Using the star polarization we have shown that the inferred magnetic field direction from the velocity gradients yields an accurate measure of the magnetic field in the 4 kpc Sun’s neighborhood for which we can provide the test with starlight polarization. This results is suggestive that our technique can be used to determine the magnetic field in regions where we do not have stellar polarization measurements. From Section 4 we have a map of the inferred magnetic field in all directions and as a function of the relative velocity. We used Eq.5 and Eq. 6 in reverse to determine the direction of the magnetic field at every distance given the known relative velocity, producing the first map of the POS galactic magnetic field direction and intensity.

The galaxy turbulent velocity is $\sim 10 \text{ km s}^{-1}$, meaning there is a limitation to the precision on the distance estimates, beside the uncertainty to the galactic rotation curve. Hence the channels with velocity widths smaller than the turbulent velocity can not give more precise distance estimations. Here we present two channels with velocity width of 2.5 km s^{-1} and 5 km s^{-1} for the RVCG and one with velocity width of 2.5 km s^{-1} for the VChG where their distances have to be limited by the turbulent velocity. Therefore even with high spectral resolution there is a minimum error to the distance, just from the galactic turbulent properties.

When the information from thin channels is used (smaller than the turbulent velocity) is important to coarse the grading of the gradients in terms of their velocity width. Since the magnetic field is slowly variant along the LOS a simple average suffice to arrive to a measurement of a coarse measurement. This measurement is the one that can be use to determine distances using this approach. In the case the original information is already form a coarse grading (channel width bigger than the turbulent velocity) then the method can be directly applied.

Figure 4 shows the inferred galactic magnetic field from the VGT. The shown magnetic field direction is the LOS-integrated direction rather than a local measurement, such that it can be compared with observations. The

map shown in Figure 4 is for the smallest channel width (10 km s^{-1}) that would give the highest resolution distance information.

The velocity gradient in the YL17 implementation gives with high accuracy the direction of the magnetic field in conditions where there the primary driver of the gas motions is turbulence. Most of the numerical studies of the technique has been done with the sub-Alfvénic turbulence. However, results in LY18 show that low-k spacial filtering provides a way for studying super-Alfvénic turbulence. In the presence of gravity, the VGT has to be modified to take into account such motions (Yuen & Lazarian 2017a; Lazarian & Yuen 2018). Additional modifications may be important in the vicinity of around spiral arms, the galactic center, and high velocity clouds.

When doing the transformation between the relative velocities and distances we assumed a galactic rotation curve. This was done throughout the whole galaxy, without any remarks on the vertical height away from the plane of the galaxy. We can therefore expect that distance estimations in the halo of the galaxy are subject to uncertainties (Figure 4). At the same time, most of the stars used in our analysis are in the galactic plane and therefore the distance estimations and AM should be accurate.

6. DISCUSSION

6.1. Requirements for using velocity gradients

The requirement for the use of velocity gradients is that the media should be turbulent. Turbulence is, however, a natural state of astrophysical fluids that are characterized by high Reynolds numbers.

It is important that one does not need to “believe” in the existence of turbulence in the media that we apply our technique. Studies of galactic HI using different tools testify of the turbulent nature of the medium (see Lazarian & Pogosyan 2000; Chepurnov & Lazarian 2010). A similar approach can be used to justify the application of our technique to other media. For instance, the turbulent spectra of ^{13}CO were measured in Padoan et al. (2009) using the Velocity Coordinate spectrum technique (see more examples in Lazarian 2009).

6.2. 3D and 2D information available with velocity gradients

All earlier attempts to employ velocity gradients have been focused on obtaining the 2D POS information on the magnetic field distribution (see YL17, LY18). The limitations of this approach stem from the fact that the line of sight additions of velocity gradient are different from the Stokes parameters and this limits the extend to which the directions obtained with polarization and magnetic field can be compared.

More importantly, it is very valuable to obtain the 3D information on the distribution of magnetic field. The rough map of 3D distribution of HI in space is available using the galactic rotation curve. Using the new tools, i.e. VChGs and RVCGs (LY18) we are able to study magnetic field distribution as a function of the distance along the line of sight.

To test the accuracy of the new way of studying 3D magnetic field distribution we used the polarization from stars to which the distances were known. These stars

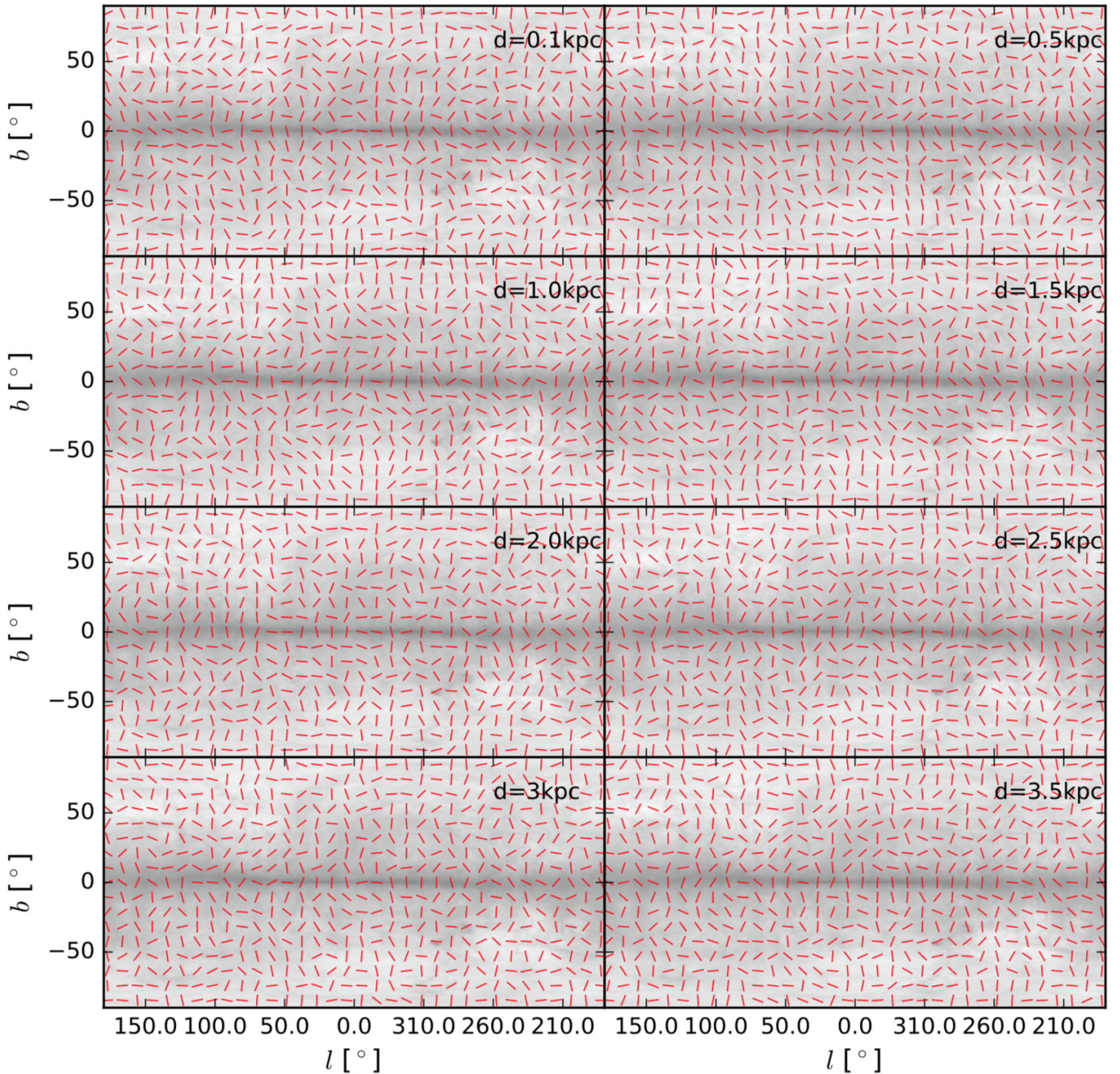


FIG. 4.— The galactic magnetic field at eight different distances from the Sun given by the different panels. The inferred magnetic field from the VGT is shown in *red* and the HI intensity map in the background. The distance are derived from the radial velocities from the spectroscopic observations assuming a galactic rotation curve.

were used as beacons to probe the accuracy of our 3D maps along the given directions. To make the corresponding comparison we used the procedure of constructing of “pseudo-Stokes” parameters as in Clark (2018). Using the stars within 4 kpc of the Sun we obtained a good correspondence between the polarization expected on the basis of our 3D maps and the actual starlight polarization. This gives us confidence that velocity gradients are able to study the 3D distribution of magnetic fields in Milky way at arbitrary distances from the observer.

We expect that the knowledge of the 3D distribution of the galactic magnetic field can help to understand key as-

trophysical processes, including the processes of star formation, propagation and acceleration of cosmic rays etc. For instance, in the process of star formation the presence of magnetic fields play a critical roll, since magnetic fields add an additional pressure acting against gravity (e.g. McKee & Ostriker 2007). The knowledge of the 3D structure of the magnetic can significantly help in understanding of the nature of this type of support.

The detailed information about magnetic field is also essential for comparing observations and MHD galactic simulations (e.g. Shetty & Ostriker 2006; Dobbs & Price 2008). The 3D information that is available with velocity gradients provide constrains on the morphology of the

field on the numerical simulations while from the simulations and affects our understanding of the transport of angular momentum as well as the pressure support in our own galaxy (Kim & Ostriker 2017).

6.3. Studies of CMB polarization

Our study also provides the way to help in the search of cosmological B-modes. These corresponding polarized signal arising from this modes is orders of magnitude less than the polarized signal from the foreground aligned galactic dust. These B-modes, if detected, would be definitive proof for inflation (Seljak & Zaldarriaga 1997).

This work presents the first measurement of the POS magnetic field embedded in the Milky Way, presenting its direction as a function of the distance from us (for the case of the disk and as a function of velocity for the halo). With this measurements both “local” (up to the turbulent velocity) and integrated along the LOS one can study the magnetic field similar to the *Planck* mission.

The *Planck* mission with the aim to understand the cosmological properties of our universe realized that it was fundamental to fully understand the local galactic imprints on their measurements, such as polarization, to derived cosmological parameters (Planck Collaboration et al. 2016a,b). Our map while lower spatial resolution it does give a 3D component of the magnetic field, this information should help constrain galactic parameters such as the polarization fraction and the magnetization that eventually will help constrain cosmological properties.

Independent of distance estimations, only analyzing the data from the VGT in velocity space, therefore no with assumptions on the rotation curve. One can identify regions where the magnetic field is highly align along the LOS. This regions would be prime candidates for CMB polarization analysis. Once this regions are detected one can use optical starlight polarization measurements with parallax the better constrain the properties of the CMB (Tassis & Pavlidou 2015).

This direction of research is similar to the one in Clark (2018) with an important distinction that we can use velocity gradients and not filaments. Elsewhere we plan to compare our technique with than in Clark (2018).

6.4. 3D distribution of media magnetization

Far-infrared polarization measurements are a common way to obtain the magnetic field direction and infer the magnetic field strength. The shortcoming of these measurements is that they suffer from instrument’s polarization, frequently require expensive space or balloon-born missions. Uncertainties of the grain alignment theory (see Lazarian & Hoang 2007) as well as the failure of grain alignment to trace magnetic field at high optical depths (Andersson et al. 2015), provide limitations for measuring magnetic field with polarimetry.

A new way of obtaining the Alfvé Mach number $M_A = V_L/V_A$, where V_L is the turbulent velocity and V_A is the Alfvé velocity is proposed in Lazarian et al. (2018). The technique is based on the fact that the distribution of velocity gradients measured within the sub-block of data points employed for the sub-block averaging depends on M_A . Within the approach that we employed in this paper the 3D distribution of M_A should be obtained.

Frequently the estimated strength of the magnetic field is derived by applying the Chandrasekhar-Fermi (C-F) method to polarization measurements (Chandrasekhar & Fermi 1953). Our approach based on velocity gradients offers a novel alternative. It was noted in GL17 that the strength of the magnetic field can also be derived using velocity gradients with a method analogous to the C-F one or via an independently derived method (Lazarian et al. 2018, GL17). The major difference is the use of the dispersion of the observed VCG instead of the dispersion of the dust polarization measurements. The estimation of the magnetic field strength has also been expanded to media with self-absorption e.g. molecular emission from CO (González-Casanova et al. 2017). In view of our present study it means that the 3D distribution of magnetic field strengths can be obtained for the galactic HI.

6.5. Complementary ways to probe the 3D magnetic field structure

We have mentioned already that the starlight polarization provides a way to probe the 3D magnetic field structure along the directions towards stars. In this paper this fact was used to test our predictions of the galactic 3D magnetic field distribution.

Another promising way is related with the use of the synchrotron polarization gradient (SPGs) (Lazarian & Yuen 2018). Magnetic turbulence induces synchrotron fluctuations the statistics of which has been recently described in Lazarian & Pogosyan (2012, 2016). The synchrotron fluctuations reflect the magnetic fluctuations. For Alfvénic turbulence the fluctuations of magnetic field and velocity enter symmetrically. Therefore it is clear that the synchrotron gradients, e.g. synchrotron intensity gradients (SIGs), are expected to trace magnetic field similar to the way velocity gradients trace magnetic field. The SIG technique was introduced in Lazarian et al. (2017). Similarly, in Lazarian & Yuen (2018) it demonstrated that the SPGs also successfully trace interstellar magnetic fields. The advantage of SPGs compared to SIGs, however, is that due to the Faraday depolarization at low frequencies the SPGs trace magnetic fields up to a certain distance along the line of sight. By changing this frequency, Lazarian & Yuen (2018) demonstrated with synthetic observations a possibility of mapping the 3D distribution of magnetic field.

In terms of the present study, the possibility of having 3D maps obtained with synchrotron is very attractive. It is important to understand that, in general, HI and synchrotron probe different phases of the ISM (see Draine 2011, for the list of the ISM phases). For many astrophysical problems, e.g. cosmic ray propagation (see Schlickeiser et al. 2007), star formation (see McKee & Ostriker 2007), it is important to know how magnetic fields in different ISM phases are interrelated.

6.6. The limitations of the approach

The velocity gradients can be evaluated at every point a local direction of the magnetic field given by the local direction of the gradient. (Yuen & Lazarian 2017b, henceforth YL17) used a statistical approach to select the peak of the distribution as the local mean magnetic field measurement. This approach provides a reliable way

to study the magnetic field direction and estimating the accuracy of the direction determination.

The limitation of using sub-block averaging is the decrease of the map resolution. The numerical studies show that the blocks of 30-60 elements may be sufficient to obtain a good Gaussian fit (see LY18). This means the decrease of the resolution of the magnetic field maps by a factor from 5 to 8 compared to the original spectroscopic maps. With high resolution instruments available, this decrease is a reasonable price to pay for obtaining magnetic field structure.

Our present study provides the 3D distribution of POS magnetic field. As we discussed, the accuracy of obtaining the distance along the line of sight depends on the profile determined by the rotation curve in the given direction. The coarse gridding is determined by the uncertainty associated with turbulent dispersion.

7. CONCLUSION

In this work we constructed the first map of the galactic magnetic field using two techniques that make use

of velocity gradients, namely, Velocity Channel Gradients (VChG) and Reduced Velocity Centroid Gradients (RVCG). The techniques were applied to the HI LAB survey. Both techniques allow the measurement of the POS magnetic field as a function of the relative velocity. Using a galactic rotation curve we transformed the relative velocity measurements to distance estimations (in the galactic disk). With these we were able to compare the inferred magnetic field direction from the VGT to the magnetic field obtained from stellar polarization. We used 1,139 star polarization measurement from the Heiles (2000) catalog to test our 3D magnetic field maps. The alignment between the two measurements was quantified and our results testify that our derived 3D galactic magnetic field map provide an accurate description of the actual galaxy magnetic field distribution.

We thank Julie Davis and Zach Pace for the insightful discussions. We particularly thank Ka Ho Yuen for the suggestions related to the data analysis. Travel support by NSF ACI 1713782 is acknowledged. Partial support for DFGC was provided by CONACyT (Mexico).

REFERENCES

- Andersson, B.-G., Lazarian, A., and Vaillancourt, J. E. 2015, *ARA&A*, 53, 501 [1](#), [6.4](#)
- Armstrong, J. W., Rickett, B. J., and Spangler, S. R. 1995, *ApJ*, 443, 209 [1](#)
- Arnal, E. M. et al. 2000, *A&AS*, 142, 35 [2.1](#)
- Bajaja, E. et al. 2005, *A&A*, 440, 767 [2.1](#)
- Chandrasekhar, S. and Fermi, E. 1953, *ApJ*, 118, 113 [6.4](#)
- Chepurnov, A. and Lazarian, A. 2010, *ApJ*, 710, 853 [1](#), [6.1](#)
- Cho, J. and Vishniac, E. T. 2000, *ApJ*, 539, 273 [1](#)
- Clark, S. E. 2018, *ApJ*, 857, L10 [4](#), [6.2](#), [6.3](#)
- Clark, S. E. et al. 2015, *Phys. Rev. Lett.*, 115 [1](#)
- Clark, S. E., Peek, J. E. G., and Putman, M. E. 2014, *ApJ*, 789 [1](#)
- Clemens, D. P., Pinnick, A. F., Pavel, M. D., and Taylor, B. W. 2012, *ApJS*, 200, 19 [4](#)
- Crutcher, R. M. 2012, *ARA&A*, 50, 29 [1](#)
- Crutcher, R. M. et al. 2010, *ApJ*, 725, 466 [1](#)
- Dobbs, C. L. and Price, D. J. 2008, *MNRAS*, 383, 497 [6.2](#)
- Draine, B. T. 2011, *Physics of the Interstellar and Intergalactic Medium* (Princeton University Press) [6.5](#)
- Elmegreen, B. G. and Scalo, J. 2004, *ARA&A*, 42, 211 [1](#)
- Esquivel, A. and Lazarian, A. 2005, *ApJ*, 631, 320 [1](#)
- Fissel, L. M. et al. 2016, *ApJ*, 824 [1](#)
- Gaia Collaboration et al. 2018, *ArXiv e-prints* [3](#), [4](#)
- Goldreich, P. and Sridhar, S. 1995, *ApJ*, 438, 763 [1](#)
- González-Casanova, D. F. and Lazarian, A. 2017, *ApJ*, 835, 41 [1](#), [3](#), [4](#), [6.4](#)
- González-Casanova, D. F., Lazarian, A., and Burkhart, B. 2017, *ArXiv e-prints* [6.4](#)
- Hartmann, D. and Burton, W. B. 1997, *Atlas of Galactic Neutral Hydrogen*, 243 [2.1](#)
- Heiles, C. 2000, *AJ*, 119, 923 ([document](#)), [1](#), [2.2](#), [1](#), [7](#)
- Kalberla, P. M. W. et al. 2005, *A&A*, 440, 775 [2.1](#)
- Kim, C.-G. and Ostriker, E. C. 2017, *ApJ*, 846, 133 [6.2](#)
- Lazarian, A. 2009, *Space Sci. Rev.*, 143, 357 [1](#), [6.1](#)
- Lazarian, A., Andersson, B.-G., and Hoang, T. 2015, *Grain alignment: Role of radiative torques and paramagnetic relaxation*, 81 [1](#)
- Lazarian, A. and Hoang, T. 2007, *MNRAS*, 378, 910 [6.4](#)
- Lazarian, A. and Pogosyan, D. 2000, *ApJ*, 537, 720 [1](#), [3](#), [6.1](#)
- . 2012, *ApJ*, 747, 5 [6.5](#)
- . 2016, *ApJ*, 818, 178 [6.5](#)
- Lazarian, A. and Vishniac, E. T. 1999, *ApJ*, 517, 700 [1](#), [1](#)
- Lazarian, A. and Yuen, K. H. 2018, *ApJ*, 853, 96 [1](#), [3](#), [5](#), [6.2](#), [6.5](#), [6.6](#)
- Lazarian, A. et al. 2018, *ArXiv e-prints* [1](#), [3](#), [6.4](#)
- Lazarian, A., Yuen, K. H., Lee, H., and Cho, J. 2017, *ArXiv e-prints* [6.5](#)
- Luri, X. et al. 2018, *ArXiv e-prints* [3](#), [4](#)
- Maron, J. and Goldreich, P. 2001, *ApJ*, 554, 1175 [1](#)
- McClure-Griffiths, N. M. and Dickey, J. M. 2007, *ApJ*, 671, 427 [4](#), [4](#)
- McKee, C. F. and Ostriker, E. C. 2007, *ARA&A*, 45, 565 [1](#), [6.2](#), [6.5](#)
- Naab, T. and Ostriker, J. P. 2016, *ArXiv e-prints* [1](#)
- Padoan, P., Juvela, M., Kritsuk, A., and Norman, M. L. 2009, *ApJ*, 707, L153 [6.1](#)
- Perryman, M. A. C. et al. 1997, *A&A*, 323, L49 [2.2](#)
- Planck Collaboration et al. 2016a, *A&A*, 594, A1 [1](#), [6.3](#)
- . 2016b, *A&A*, 594, A10 [1](#), [6.3](#)
- Schlickeiser, R., Dohle, U., Tautz, R. C., and Shalchi, A. 2007, *ApJ*, 661, 185 [6.5](#)
- Seljak, U. and Zaldarriaga, M. 1997, *Physical Review Letters*, 78, 2054 [6.3](#)
- Shetty, R. and Ostriker, E. C. 2006, *ApJ*, 647, 997 [6.2](#)
- Soler, J. D. et al. 2017, *A&A*, 603, A64 [1](#)
- . 2016, *A&A*, 596, A93 [4](#)
- . 2013, *ApJ*, 774, 128 [1](#)
- Tassis, K. and Pavlidou, V. 2015, *MNRAS*, 451, L90 [6.3](#)
- Yuen, K. H. and Lazarian, A. 2017a, *ArXiv e-prints* [5](#)
- . 2017b, *ApJ*, 837, L24 [1](#), [3](#), [3](#), [3](#), [5](#), [6.2](#), [6.6](#)